ELECTRICAL AND OPTICAL CHARACTERIZATION OF NANOSTRUCTURES

E. GORNIK, J. SMOLINER AND V. ROSSKOPF

Technische Universität Wien, Institut für Festkörperelektronik 362
Gußhausstraße 25-29, 1040 Wien, Austria

The characterization of nanostructures is a topic of vital interest, since the dimensions of commercially available semiconductor devices are now in a range, where quantum size effects become evident. In this paper, various methods are presented to characterize low-dimensional structures. Magnetic depopulation, tunneling, far infrared transmission, photo-conductivity and magnetophonon resonances are used to determine the low-dimensional sub-band energies. For each method, the special features are discussed and it is demonstrated that the different methods yield different, complementary information.

PACS numbers: 73.20.Dx

1. Introduction

The crucial parameter to characterize low-dimensional structures is the sub-band spacing between the one- (1D) or zero-dimensional (0D) subbands. The classic experiment to investigate 1D structures, which are also called quantum wires, is a magnetic depopulation experiment, which was first performed by Berggren et al. on a split gate field effect transistor. Assuming a parabolic electrostatic confinement, the influence of an additional magnetic field can be analyzed analytically. It was shown that the additional magnetic field increases the subband spacing so that the 1D subbands are shifted above the Fermi energy if the magnetic field is increased. Consequently the 1D subbands are depopulated resulting in an oscillatory behavior of the magnetoresistance. In contradiction to the 2D case, a plot of the oscillation index versus the inverse magnetic field $1/B$ (Landau plot) is not linear and saturates at low magnetic fields. By fitting the experimental data both the 1D electron concentration and the 1D subband spacing is obtained. From this, the widths of the 1D channels can also be calculated. Since the simple harmonic oscillator model is not always sufficient to explain the experimental results, modified potentials [1, 2], density of state effects and the influence of lifetime broadening due to scattering processes were also taken into account. Alternatively to the above method, the 1D subband energies can also be extracted from Dingle plots [3] or

the non-linear behavior of the magnetoconductance at very low magnetic fields [4] or far infrared transmission measurements [5–8].

In the present paper, different characterization methods, such as magnetotransport, tunneling, magnetophonon resonances, FIR (far infrared radiation) transmission and photo-conductivity measurements are used to investigate the 1D subband spacings of low-dimensional structures fabricated on GaAs–GaAlAs heterostructures. It is shown that each method has its individual advantages and it is also demonstrated that the obtained results yield different, complementary information.

2. Sample preparation

The samples, which are typically used for all the presented experiments, consist of an unintentionally p-doped GaAs layer grown on a semi-insulating substrate ($N_A < 10^{14}$ cm^{-3}), followed by an undoped spacer ($d = 100$ Å), and doped Al$_x$Ga$_{1-x}$As ($d = 250$ Å, $N_D = 4 \times 10^{18}$ cm^{-3}, $x = 0.3$). The additional GaAs cap layer is highly n-doped ($d = 150$ Å, $N_D = 5.7 \times 10^{18}$ cm^{-3}). Bar-shaped mesas were etched into the sample and ohmic contacts were aligned using an AuGe alloy. Then, laser holographic gratings having a period of typically 400 nm, were fabricated on the samples. The length of the wires was $l = 100$ μm for all samples. The photoresist patterns are transferred into the GaAs by wet chemical etching (H$_2$O:H$_2$O$_2$:NaOH=1:300:500). Two different samples were prepared. Sample 2 was etched for 30 s and sample 1 was etched for 45 s. Thus, the subband spacing is expected to be higher for sample 1. The mobility of the unstructured samples was $\mu = 3.8 \times 10^5$ cm^2/(V s) and the electron density was 6.2×10^{11} cm^{-2} at $T = 4.2$ K. A schematic view of the samples is shown in Fig. 1.

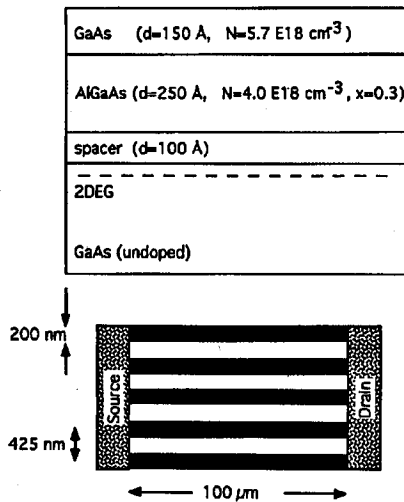Fig. 1.   Schematic view of the sample.

3. Magnetic depopulation

To characterize the properties of these wires, magnetoresistance measurements were performed in a configuration where the magnetic field is applied perpendicular to the multiple wire structure. Typical experimental data are shown in the inset of Fig. 2. At low temperatures ($T = 3$ K) Shubnikov–de Haas (SDH) oscillations are observed above $B = 1$ T. The peak around 0.5 T is due to situation where the cyclotron diameter matches the width of the wire [9].
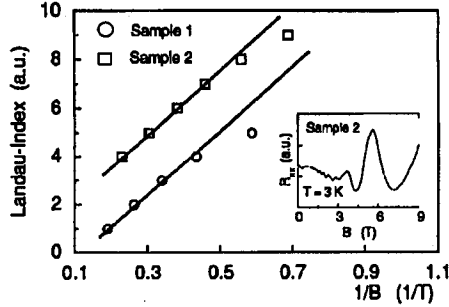

Fig. 2. Landau plot of the experimental peak positions. The inset shows the corresponding magnetotransport data.

A Landau plot was used to evaluate the subband spacings in the one-dimensional systems. To extract the subband spacing and the 1D electron concentration in the quantum wires from this plot, a simple harmonic oscillator model is used. The equidistant 1D subband energies in an external magnetic field are given by

$$E_n = \hbar\Omega \left(n + \frac{1}{2} \right) + \frac{\hbar^2 k_y^2}{2m^*(B)}, \tag{1}$$

where $\Omega^2 = \omega_c^2 + \Omega_0^2$, $m^*(B) = (\Omega^2/\Omega_0^2)m^*$ and ω_c is the cyclotron frequency. Thus the subbands are separated by $\hbar\Omega$. The positions of the observed magnetoresistance oscillations were calculated using a two parameter fit (n_{1D}, Ω_0), taking the 1D density of states into account. By this procedure, the deviation from the linear behavior yields subband spacings of $\hbar\Omega_0 = 2.5$ meV for sample 1 and $\hbar\Omega_0 = 1.0$ meV for sample 2, respectively. Note that these results are consistent with the higher etching times for sample 1.

4. 3D–1D tunneling

To measure the subband spacing directly, tunneling measurements were performed. For this purpose, an Au-gate was evaporated on the samples. The rest of the fabrication process was the same. On such a sample, the $I(V_G)$ and dI/dV_G curves were measured between the gate contact and the quantum wire system using a high resolution, 4-terminal conductance bridge. Figure 3 shows the dI/dV_G curves of two samples having different grating periods and therefore different geometrical widths of the quantum wires. A series of equidistant peaks is evident in all
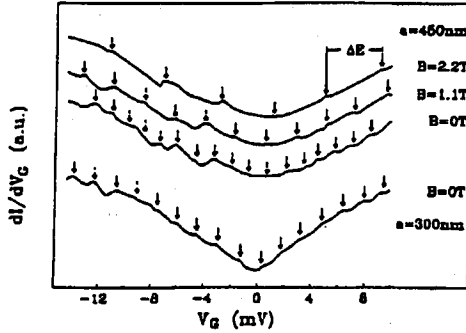
Fig. 3. dI/dV_G curves measured on samples with grating periods of 450 nm and 300 nm.

curves, where at $B = 0$ T, the observed structures are larger for the 300 nm sample. With increasing magnetic field, the spacing between the peaks is also increased.

All these effects are well explained by the harmonic oscillator model, assuming that the equidistant structures in the dI/dV_G curves occur each time the Fermi energy in the metal gate (3D electrons) crosses a subband in the quantum wires (1D system). As the measurement is performed in a very small bias range, the subband spacing can be assumed to be constant and therefore the energy spacing ΔE between the subbands is simply $e\Delta V_G$. To check this assumption, the magnetic field data can be used. With increasing magnetic field, the spacing between the peaks increases. The increase in the spacing is quantitatively explained by the contribution of the magnetic field to the subband energy, and thus, tunneling turns out to be a simple and helpful tool to determine the 1D subband spacings on gated quantum wires, which yields equivalent results compared to the magnetic depopulation measurements [10].

5. 1D–2D tunneling

Although tunneling works well on the above samples, much more beautiful results can be achieved on a system, where tunneling takes place between a 2DEG (two-dimensional electron gas) and a multiple quantum wire system separated by a thin barrier. These samples consist of a nominally undoped GaAs layer ($N_A \leq 1 \times 10^{14}$ cm^{-3}) grown on a semi-insulating substrate, followed by an undoped spacer ($d = 50$ Å), doped AlGaAs ($d = 50$ Å, $N_D \leq 3 \times 10^{18}$ cm^{-3}, $x = 0.36$) another spacer ($d = 100$ Å) and n-doped GaAs ($d = 800$ Å, $N_D \leq 1.2 \times 10^{15}$ cm^{-3}). An additional GaAs cap layer was highly n-doped ($d = 150$ Å, $N_D = 6.4 \times 10^{18}$ cm^{-3}). This structure provides an inversion layer at the lower GaAs/AlGaAs interface, containing several 2D subbands, and an accumulation layer at the upper AlGaAs/GaAs interface, separated by a barrier of only 200 Å thickness. From Shubnikov–de Haas measurements it was deduced that in both 2DEG systems only one subband is occupied with values of $n_s^{inv} = 6.0 \times 10^{11}$ cm^{-2} and $n_s^{acc} = 5.5 \times 10^{11}$ cm^{-2} for the electron densities, respectively.

As earlier, a multiple quantum wire system was fabricated on the samples using standard laser holographic techniques. The wires were etched wet chemically

300 Å deep into the GaAs, depleting locally the upper electron system, but leaving the lower inversion channel untouched. This is shown schematically in Fig. 4a. By applying a voltage V_b, the 1D-states are shifted energetically by $\Delta E = eV_b$ with respect to 2D-electron gas, since this external electric field drops completely across the potential barrier [11]. The corresponding band structure, which illustrates this situation, is shown in Fig. 4b. All transitions between these states of different dimensionality are reflected in the tunneling current, allowing to obtain information about the 1D-quantization energies as well as about the confining potential.
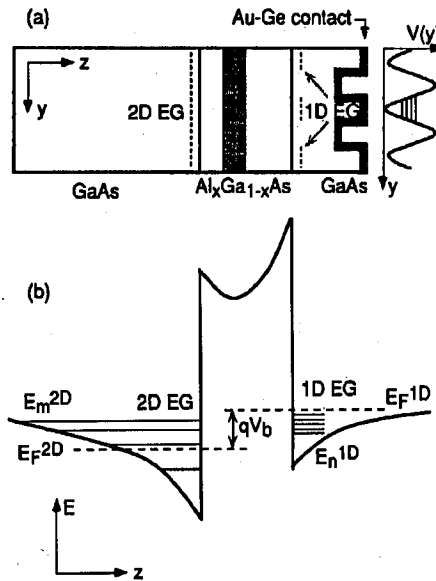

Fig. 4.   (a) Schematic view of the samples. (b) Corresponding conduction band profile.

In the case of an unstructured sample, resonant tunneling between the two 2DEG systems is reflected in a series of sharp peaks in the dI/dV_b characteristic, as shown in Fig. 5a, curve 1 for low temperatures. In this geometry, the electrons transverse momentum (with respect to the tunneling current) is conserved during the tunneling process. Resonant tunneling occurs each time the subband in the accumulation layer matches energetically a subband in the inversion layer [12, 13]. With increasing temperature up to $T = 30$ K all structures remain almost unchanged. For even higher temperatures, the resonance position at negative bias voltages start to shift to even more negative values. In Fig. 5a, curve 2 shows the dI/dV_b characteristic at $T = 50$ K. Beside shifting, the peak width increases as their amplitude decreases.

The corresponding dI/dV characteristic of the nanostructured sample is plotted in Fig. 5b, curve 1. It exhibits extremely rich and well observable structures within the investigated bias voltage regime. In our previous work, these peaks were related to resonances between the edges of the 2D subbands in the inversion layer
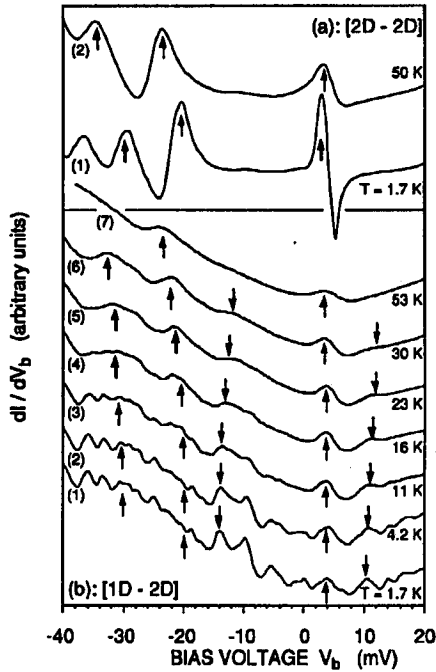
Fig. 5.   Typical dI/dV curves of an unstructured 2D–2D (a) and a nanostructured sample (b).

and the 1D states in the quantum wire system [14]. Note that these new resonance structures exist even at low values of V_b. Therefore resonant tunneling is allowed as soon as there is a difference in the Fermi energies between both sides of the barrier.

   In order to gain more information about the selection rules of the 1D to 2D tunneling process, we analyze the temperature dependence of these transitions. The characteristics for temperature values between 1.7 K and 53 K are shown in Fig. 5b, curves 2 to 7. The curves traced at low temperatures exhibit extremely rich structures. As the temperature rises up to $T = 15$ K, the peak amplitudes decrease monotonically, whereas the linewidth remains unaffected, as expected in the case of resonant tunneling. Within the bias voltage range between $V_b = -15$ and $+ 3$ mV, however, the structures vanish more rapidly with increasing temperature. Above $T = 23$ K, only a few structures remain resolved. The arrows pointing upwards mark the resonance positions of the unstructured sample. For $T \geq 50$ K, the positions of the three remaining resonance structures are at bias voltages of -32 mV, $V_b = -23.5$, and $+ 4.0$ mV, which correspond to the resonance positions for tunneling transitions between the subband of the non-nanostructured accumulation layer and the three lowest subbands of the inversion layer (Fig. 5a, curve 2). The high temperature characteristics of the nanostructured sample therefore show a 2D–2D like behavior.

To analyze these data quantitatively, a transfer Hamiltonian formalism was developed and it was shown that the tunneling current is directly proportional to the wave function overlap between the 1D and 2D system. The main results can be summarized as follows. First, structures in the tunneling characteristics are not only observed, when a 2D subband matches a 1D subband. This is only true for even 1D subband indices. For odd 1D subband, the structures in the tunneling characteristics are shifted by a voltage ΔV_n with respect to the voltage position V_n, where the subbands coincide. This is illustrated in Fig. 6 where the
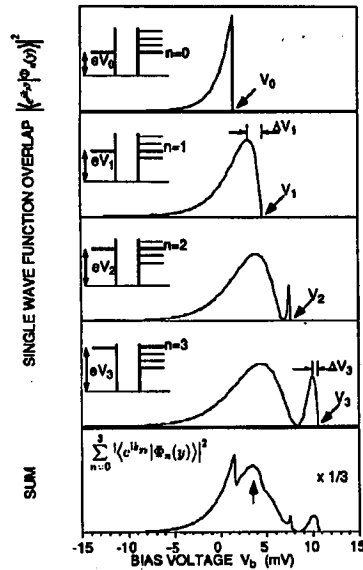

Fig. 6.   Wave function overlap between the 1D and 2D side is plotted for the four lowest 1D subbands.

wave function overlap between the 1D and 2D side is plotted for the four lowest 1D subbands. Second, there is an additional structure in the tunneling current at off resonance bias, which is also due to the wave function overlap as a function of the applied bias voltage. Third, the positions of these extra peaks and their temperature behavior are extremely sensitive to the shape of the potential. It was found that the experimental data can only be explained if a cosine shaped potential is used for the quantum wires. Parabolic or rectangular potentials yield completely different results and are therefore not suitable to describe the potential in this quantum wire system. Finally, the subband spacings on this special sample are much higher than in quantum wires realized on normal heterostructures. This effect is most probably due to the special fabrication process of the top contacts. If optimized, one could reach the quantum limit and then, this geometry of a 1D to 2D tunneling transition offers a very elegant possibility to perform *wave function spectroscopy*.

6. Far infrared radiation (FIR) spectroscopy

Much insight into the electronic properties of low-dimensional electron systems is gained from investigations of their FIR excitations. A good review on these techniques is given in Ref. [15]. It was demonstrated in etched [16] as well as field-effect [17] induced low-dimensional electron systems that the bare confinement V_{ext} has parabolic shape in very good approximation. Taking the generalized Kohn theorem [18] into account, the FIR conductivity exhibits a single-dimensional resonance at a frequency that corresponds to the characteristic frequency of this bare potential. The meaning of "bare potential" here is that the potential is induced by all external charges contributing to the confinement as e.g. charges on the gate pattern, in surface states or image charges on the semiconductor interfaces, but not by the electrons that occupy the quantum wire. Experiments [19] and model calculations demonstrate that 1D electron systems are usually smaller than the lithographically defined patterns on the surface. Therefore, once the wires in a superlattice are defined, they can be regarded as decoupled in a very good approximation with wide barriers between them.

In Fig. 7 the experimental FIR spectra of an one layered shallow etched quantum wire structure based on a quantum well sample is shown. For comparison, a non-structured sample is also shown. The transmission measurements were
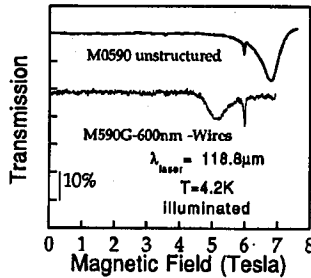

Fig. 7.   Transmission spectra of a quantum wire sample. For comparison, a reference spectrum is also shown.

performed using a FIR laser, with fixed wavelength of 118.8 μm. On the structured sample, the resonance position is shifted to lower magnetic fields with respect to the non-structured sample, which means that it is shifted to higher resonance energies. The spectra also exhibit a second, very sharp resonance, that does not change its position. This resonance is due to a parasitic 2D electron inversion channel below the structured quantum well, which is not affected by the shallow etching process. Thus, this line can be used for reference purposes. Assuming a parabolic potential V_{ext}

$$V_{ext} = \frac{1}{2} m^* \omega_0^2 x^2 \tag{2}$$

and in the presence of a magnetic field B the characteristic frequency ω can be derived analytically using classical or quantum mechanical methods
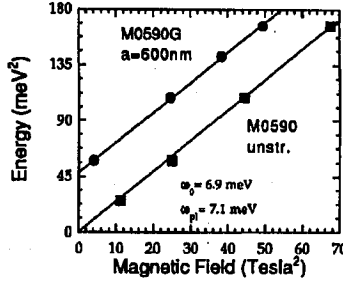
$$\omega = \sqrt{\omega_0^2 + \omega_c^2}. \tag{3}$$

Fig. 8. Squared resonance energy ω^2 plotted against the squared magnetic field B^2.

Here ω_0 denotes the cyclotron resonance frequency eB/m^*. Plotting of the squared resonance energy ω^2 against the squared magnetic field B^2 (Fig. 8) for different laser lines, results in a linear dependence giving ω_0 at $B = 0$. According to the very good agreement between theoretical and experimental data, the parabolic approximation of the bare potential is verified.

Another method to characterize low-dimensional electrons systems are FIR photoconductivity measurements. By lock-in amplifier techniques the difference signal between FIR-illuminated and non-illuminated in the conductivity is recorded. In analogy to transmission measurements, photoconductivity also yields the unscreened potential, but has several advantages. First, samples with much smaller structured areas can be investigated than in transmission geometry, where large samples have to be used. In the extreme case, it is even possible to measure the photoconductivity of only a single quantum wire. Due to a much larger sensitivity, high temperature measurements can also be performed. Latest measurements of the temperature dependence of the photoconductivity of a quantum wire array show that the resonance position does not shift with temperature from 1.5 K up to 80 K, only the height of amplitude decreases strongly and the width is broadening with increasing temperature. This means that in the whole range between $T = 1.8$ K and $T = 80$ K, the shape of the potential is almost insensitive to the temperature of the sample.

7. Magnetophonon resonances

In the past, magnetophonon resonances were intensively studied in two-dimensional systems to determine the polaron mass [20]. In addition to magneto-transport experiments, magnetophonon resonances are also investigated by cyclotron resonance measurements [21, 22], where it was possible to determine the energy relaxation rates. In recent systematic measurements [23], magnetophonon resonances in two-dimensional electron gas were studied as a function of temperature, electron concentration and magnetic field orientation. Theoretical considerations on magnetophonon resonances for two-dimensional electron systems were performed by Hamaguchi et al. [24] and Mori et al. [25]. Most recently, magnetophonons were also observed in vertical transport experiments performed on GaAs–AlGaAs superlattices [26].

For nanostructured systems, such as quantum wires, interesting magneto-phonon effects were already predicted theoretically [27–30] but there are only few experimental hints that phonons play an important role in nanostructures [31], such as quantum-wire structures [32].

In this part of the paper we analyze the magnetotransport properties of quantum wires at high temperatures ($T \approx 150$ K). The energy spacing of the 1D structure and the polaron mass is obtained from the experimental data and it is shown that in the case of a 1D system, the polaron mass is higher compared to the bulk GaAs value.

The experimental data are shown in Fig. 9. For temperatures around $T = 100$ K the Shubnikov–de Haas oscillations, which are dominant at liquid helium temperatures, are washed out. At even higher temperatures (T approximately 130–180 K) additional structures are observed in the magnetoresistance R_{xx}, which are associated with magnetophonon resonances. The maxima observed in Fig. 9 for $T = 150$ K at magnetic fields of $B = 7$ T, $B = 4.5$ T and $B = 2.8$ T represent these effects. For even higher temperatures the oscillations disappear.
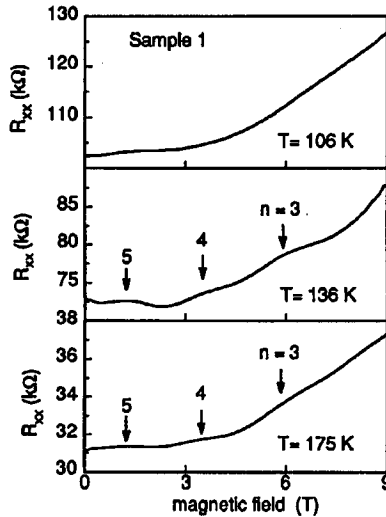

Fig. 9.   Magnetoresistance curves measured at $T = 100$ K, $T = 136$ K and $T = 175$ K.

To analyze the experimental data quantitatively, we assume a parabolic con-finement $V(y)$ for the quantum wires with $V(y) = 1/2m^* \Omega_0^2 y^2$, where y is the direction perpendicular to the wire, m^* is the electron effective mass (or polaron mass) and Ω_0 describes the strength of the electrostatic potential. The correspond-ing subband spacing at $B = 0$ T is given as $\hbar\Omega_0$. Magnetoresistance maxima are expected each time, an integer (n) multiple of the 1D subband spacing is equal to the LO-phonon energy (see Eq. (1)).

$$n\hbar\sqrt{\omega_c^2 + \Omega_0^2} = \hbar\omega_{\text{LO}}. \tag{4}$$

Rewriting Eq. (1) in terms of B^2, we obtain

$$B^2 = \left(\frac{m^* \omega_{LO}}{e}\right)^2 \frac{1}{n^2} - \left(\frac{m^* \Omega_0}{e}\right)^2 . \tag{5}$$

If we consider the 2D case, which means $\Omega_0 = 0$, we obtain the usual magneto-phonon peak positions, which are equidistant in $1/B$. Further, the polaron effective mass, m^*, can be determined from the slope of the curve, if the phonon energy is known or vice versa. In the case of a nanostructured sample, which means $\Omega_0 > 0$, the curve intersects the B^2-axis no longer at $B = 0$, which offers the possibility to determine the 1D subband energies from the magnetophonon peak positions. Note that in contrast to magnetic depopulation measurements, this method offers the possibility to measure the subband spacing for samples, which are in the extreme quantum limit at low temperatures, where SDH oscillations cannot be observed.

Figure 10 shows the results of the above considerations, where we have plotted the magnetophonon peak positions in B^2 vs. $1/n^2$. The peak positions for the two electron densities follow the predicted linear behavior in good agreement with the theoretical predictions. The slope of the linear dependence of B^2 vs. $1/n^2$ in Fig. 10 can be used to determine the polaron mass m^* of the electrons in the quantum wire. If we assume the bulk GaAs LO phonon energy, the polaron mass of
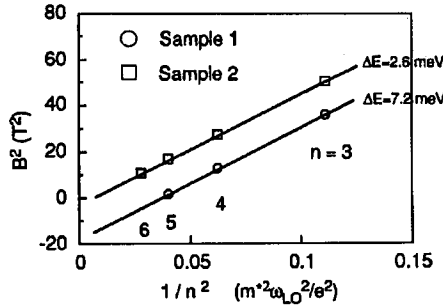

Fig. 10. Magnetophonon peak positions in B^2 plotted as a function of $1/n^2$.

about $m^* = 0.08$ (± 0.005) is obtained. Values of the polaron mass m^* determined by magnetophonon effect in bulk GaAs and 2D systems do not exceed m_{eff} by more than 10%. Thus we can conclude that in the studied 1D system the polaron mass m^* is larger than m_{eff} in bulk GaAs by about $20 \pm 5\%$. Using the polaron mass m^* we now determine the subband spacing from the intersection with the B^2 axis due to formula (2) for a one-dimensional electron system. By this procedure, we obtain values of 2.6 meV and 7.2 meV, which are more that a factor of 2 larger than the results obtained by low temperature magnetotransport and the tunneling data.

The reason for this is still unclear. Several possibilities exist. First, the 1D subband spacing changes drastically at high temperatures. This assumption is not easy to verify, since magnetophonon resonances are the only tool to determine 1D subband spacings at such high temperatures. Further, there is almost no tempera-ture dependence of the resonance peaks between $T = 106$ K and $T = 175$ K, which

means that the subband spacing does not depend on the temperature in this range. FIR-photoconductivity measurements up to 80 K also indicate that there is almost no temperature dependence of the subband energies, and yield subband spacings of the unscreened potential, which are still lower than the magnetophonon data. Second, the magnetophonon also measure an unscreened potential at high temperature as it is the case for the FIR measurements. However, there is no theoretical reason for this until now. Third, the model is incomplete in the present form, and additional selection rules have to be taken into account.

8. Summary

In summary, several methods were presented to characterize 1D systems. At low temperature, magnetotransport and tunneling yield equivalent results. Tunneling however is more flexible and can be used to extract additional information on the shape of the potential. In contrast to the electrical methods, FIR-measurements always yield the unscreened potential. Comparing these results with the magnetotransport or tunneling data, this is a useful tool to study the influence of the electron concentration in the system. High temperature measurements are still somewhat problematic in present nanostructures where the subband spacing is well below kT at room temperature. However, all techniques of tunneling, magnetotransport and FIR photoconductivity can be extended up to room temperatures for devices with subband energies in the 20 meV range and can thus be used to study the basic properties of future nanodevices designed for high temperature use.

Acknowledgments

References

[1] K.F. Berggren, D.J. Newson, *Semicond. Sci. Technol.* 1, 327 (1986).

[3] H.J. Rundquist, *Semicond. Sci. Technol.* 4, 455 (1989).

[3] H. Lakrimi, A.C.D. Grassie, K.M. Hutchings, J.J. Harris, C.T. Foxxon, *Semicond. Sci. Technol.* 4, 313 (1989).

[4] T.J. Thornton, M. Pepper, H. Ahmed, D. Andrews, G.J. Davies, *Phys. Rev. Lett.* 56, 1198 (1986).

[5] F. Brinkop, W. Hansen, J.P. Kotthaus, K. Ploog, *Phys. Rev. B* 37, 6547 (1988).

[6] J. Alsmeier, Ch. Sikorski, U. Merkt, *Phys. Rev. B* 37, 4314 (1988).

[7] W. Hansen, M. Horst, J.P. Kotthaus, U. Merkt, Ch. Sikorsky, K. Ploog, *Phys. Rev. Lett.* 58, 2586 (1987).

[8] T. Demel, D. Heitmann, P. Grambow, K. Ploog, *Phys. Rev. B* 38, 12732 (1989).

[9] T.J. Thornton, M.L. Roukes, A. Scherer, B.P.van de Gaag, *Phys. Rev. Lett.* 63, 2128 (1989).

[10] F. Hirler, J. Smoliner, E. Gornik, G. Weimann, W. Schlapp, *Appl. Phys. Lett.* 57, 261 (1990).

[11] J. Smoliner, W. Demmerle, F. Hirler, E. Gornik, G. Weimann, M. Hauser, W. Schlapp, *Phys. Rev. B* **43**, 7358 (1991).

[12] J. Smoliner, W. Demmerle, G. Berthold, E. Gornik, G. Weimann, W. Schlapp, *Phys. Rev. Lett.* **63**, 2116 (1989).

[13] W. Demmerle, J. Smoliner, G. Berthold, G. Weimann, W. Schlapp, *Phys. Rev. B* **44**, 3090 (1991).

[14] J. Smoliner, F. Hirler, E. Gornik, G. Weimann, M. Hauser, W. Schlapp, *Semicond. Sci. Technol.* **6**, 389 (1991).

[15] For a review see W. Hansen, J.P. Kotthaus, U. Merkt, *Semicond. Semimetals* **35**, 279 (1990).

[16] T. Demel, D. Heitmann, P. Grambow, K. Ploog, *Superlattices Microstruct.* **9**, 285 (1991).

[17] W. Hansen, in: *Proc. NATO ASI Quantum Coherence in Mesoscopic Systems*, Ed. B. Kramer, Series B, Vol. 254, Plenum Press, New York 1991, p. 23.

[18] S.K. Yip, *Phys. Rev. B* **43**, 1707 (1991) and references therein.

[19] R. Strenz, V. Rosskopf, F. Hirler, G. Abstreiter, E. Gornik, G. Böhm, G. Weimann, to be published.

[20] D.C. Tsui, T. Englert, A.Y. Chao, A.C. Gossard, *Phys. Rev. Lett.* **44**, 341 (1980).

[21] P. Warmenbol, F.M. Peeters, X. Wu, J.T. Devreese, *Phys. Rev. B* **40**, 6258 (1989).

[22] P. Warmenbol, F.M. Peeters, J.T. Devreese, *Phys. Rev. B* **37**, 4694 (1988).

[23] M.A. Brummel, D.R. Leadley, J.R. Nicholas, J.J. Harris, C.T. Foxon, *Surf. Sci.* **196**, 451 (1988).

[24] C. Hamaguchi, N. Mori, H. Murata, K. Taniguchi, in: *High Magnetic Fields in Semiconductor Physics II*, Vol. 87, Ed. G. Landwehr, Springer, Heidelberg 1989, p. 541.

[25] N. Mori, H. Murata, K. Taniguchi, C. Hamaguchi, *Phys. Rev. B* **38**, 7622 (1988).

[26] N. Noguchi, H. Sakaki, T. Takamasu, N. Miura, *Phys. Rev. B* **45**, 12148 (1992).

[27] P. Vasilopoulous, P. Warmenbol, F.M. Peeters, J.T. Devreese, *Phys. Rev. B* **40**, 1810 (1989).

[28] N. Mori, H. Momose, C. Hamaguchi, *Phys. Rev. B* **45**, 4536 (1992).

[29] M.H. Degani, O. Hipolito, *Superlattices Microstruct.* **5**, 137 (1989).

[30] E.S. Hellman, J.S. Harris, *Phys. Rev. B* **33**, 8284 (1986); S. Briggs, B.A. Mason, J.P. Leburton, *Phys. Rev. B* **40**, 12001 (1989); V.B. Campos, M.H. Degani, O. Hipolito, *Solid State Commun.* **79**, 473 (1991).

[31] K. Ismail, *Proc. Int. Symp. on Science and Technol. of Mesoscopic Structures*, Nara, Nov. 1991, to be published.

[32] G. Berthold, J. Smoliner, M. Hauser, C. Wirner, E. Gornik, G. Böhm, G. Weimann, C. Hamaguchi, N. Mori, H. Momose, to be published.